

Jahn-Teller mediated ordering in layered Li_xMO_2 compounds

M. E. Arroyo y de Dompablo, C. Marianetti, A. Van der Ven, and G. Ceder

Department of Material Science and Engineering, Massachusetts Institute of Technology, Cambridge, Massachusetts 02139

(Received 9 October 2000; published 21 March 2001)

Lithium ordering in layered Li_xMO_2 compounds ($M = \text{Ni, Co, Mn}$) is investigated with first-principles calculations. We found that apart from the in-plane Li-Li interactions, the stability of ordered Li_xMO_2 structures strongly depends on the interlayer Li-Li interactions through the M cations. When several stacking sequences are possible, the selection of stacking is shown to be driven by the electronic structure of the transition-metal cations (metallic for $\text{Co}^{+3/+4}$, localized for $\text{Ni}^{+3/+4}$ and $\text{Mn}^{+3/+4}$). In Li_xCoO_2 the stacking is chosen so as to minimize the variations in coordination of the symmetrically different Co sites, thus enhancing electronic charge delocalization. In Li_xNiO_2 , lithium ordering couples to orbital and Jahn-Teller ordering so as to form 180° Li-O-Ni⁺³-O-Li complexes. The presence of these 180° Li_A -O- M -O- Li_B interactions ensures distinct M environments and charge localization. We indicate how the coupling between the e_g^* and Li-2s orbital hybridization and the Jahn-Teller distortion produces a long-range attractive interaction between Li ions.

DOI: 10.1103/PhysRevB.63.144107

PACS number(s): 61.50.Ah, 61.66.Fn, 71.70.-d, 64.60.Cn

I. INTRODUCTION

Ordering between cations, or between cations and vacancies, is a common phenomenon in oxides.¹ The effective interactions that drive this ordering result from a subtle balance between electrostatic and size effects. For example, in rocksalts with compositions ABO_2 , the A and B cations form the electrostatically favored α - LiFeO_2 structure when A and B have similar ionic radii.² For large radii difference the α - NaFeO_2 structure is formed as it allows for optimal relaxation of individual A -O and B -O bond lengths. Such a combination of relaxation and electrostatic effects can be used to explain many of the observed structures in multicomponent oxides. In this paper we report on ionic ordering that is driven through the orbital interaction with Jahn-Teller cations, leading to indirect but very long-range interactions. Our focus is on LiCoO_2 and LiNiO_2 in the layered α - NaFeO_2 structure.

Layered transition-metal oxides LiMO_2 ($M = \text{Mn, Ni, Co}$) have been the focus of considerable attention due to their application in lithium batteries. These compounds can be viewed as ‘‘ordered rocksalts’’ in which alternate layers of Li^+ and M^{+3} ions occupy octahedral sites within the cubic close-packed oxygen array. The lithium ions can be reversibly removed from and reinserted into this structure, creating or annihilating vacancies within the lithium planes.

When Li is removed electrochemically from LiMO_2 compounds, Li-vacancy ordering can occur, and has been observed in Li_xCoO_2 (Ref. 3) and Li_xNiO_2 (Ref. 4). First-principles calculations have confirmed the occurrence of Li-vacancy ordering in Li_xCoO_2 .⁵ Lithium and the transition-metal cations occupy alternating $\{111\}$ planes of the oxygen host. Hence, the sites in the lithium plane form a triangular network. Different lithium planes are relatively far apart (~ 5 Å) and are separated by the transition-metal layer. In this paper, we show that indirect interactions through the transition-metal layer can strongly couple the different Li layers, and that the specific electronic characteristics of the

transition metal determines the particular interlayer stacking that is adopted.

In the fully lithiated LiMO_2 compounds, the metal cation is in a +3 valence state. Hence Li removal will create a mixture of +3 and +4 cations. While Co^{+3} and Ni^{+3} have similar ionic radii they differ in electronic configuration. In these oxides Co^{+3} is low spin with $(t_{2g})^6$ configuration, whereas Ni^{+3} has $(t_{2g})^6(e_g)^1$ configuration. The degeneracy of the two e_g levels gives the Ni^{+3} potential Jahn-Teller (JT) activity. For comparison, some calculations will also be performed on low spin $(t_{2g})^4(e_g)^0$ and high spin $(t_{2g})^3(e_g)^1$ Mn^{+3} . The latter has a strong JT-active electronic configuration.

Layered LiCoO_2 crystallizes in a rhombohedral lattice that belongs to the $R\bar{3}m$ space group. Within this space group, Li occupies the $3a$, Ni the $3b$, and O the $6c$ sites.⁶ A collective Jahn-Teller distortion of the $R\bar{3}m$ structure along one of the octahedral axes can lower the symmetry to $C2/m$. This is found in layered LiMnO_2 , which is a metastable compound. In the $C2/m$ space group Li occupies the $2d$, Ni the $2a$, and O the $4i$ sites.⁷ LiNiO_2 adopts a rhombohedral symmetry at all temperatures,^{8,9} in spite of the Jahn-Teller distorted low spin Ni^{+3} ions [$(t_{2g})^6(e_g)^1$]. This fact is likely connected to the departure from stoichiometry in the prepared LiNiO_2 compounds, whereby excess Ni occupies Li sites ($\text{Li}_{1-z}\text{Ni}_{1+z}\text{O}_2$).^{9,10,11} However, local Jahn-Teller distortions have been observed with extended x-ray-absorption fine structure (EXAFS) experiments even in nonstoichiometric LiNiO_2 .¹² First-principles calculations predict that at low temperature the most stable form of stoichiometric LiNiO_2 is monoclinic distorted¹³ ($C2/m$). Therefore, in the present work we consider monoclinic LiNiO_2 as the fully lithiated compound, from which deintercalated Li_xNiO_2 is obtained.

A. Ordered structures in the two-dimensional triangular lattice

The fragment of the α - NaFeO_2 - type structure in Fig. 1 shows the lithium and metal layers surrounded by oxygen layers. These oxygens form a network of edge-sharing octa-

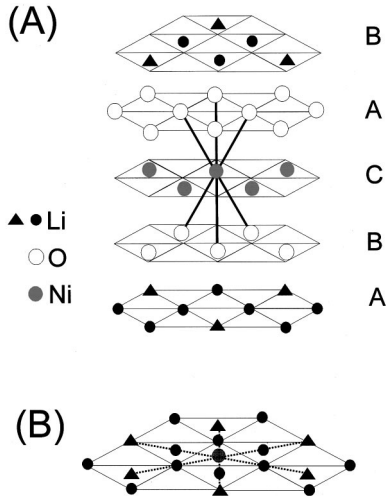


FIG. 1. (a) Schematic representation of the layered LiMO_2 structure. Lithium ions in planes A and B are denoted with solid circles or triangles. The triangles are those Li ions that are at the extension of the M -O bond from the central M ion. These Li ions form three $180^\circ \text{Li}_A\text{-O-M-O-Li}_B$ pairs with the central M ion. (b) Projection of the structure onto the basal plane showing two planes of lithium ions A and B, and the $180^\circ \text{Li}_A\text{-O-M-O-Li}_B$ interactions through the central M ion (dashed line).

hedra around the triangular planes of Li sites. Effective interactions between Li sites are expected to be repulsive and decaying with distance, as they are likely determined by screened electrostatics and some oxygen displacement. Indeed this was found in a first-principles study of the Li_xCoO_2 system.⁵ For short-range repulsive interactions, possible ground states of the triangular lattice are known^{14,15} and some are shown in Fig. 2. All the in-plane lithium-vacancy ordering observed in either Li_xCoO_2 or Li_xNiO_2 fall into those of Fig. 2, confirming the existence of short-ranged repulsive interactions. However, in-plane Li-vacancy ordering does not completely specify the structure. In most cases, different stackings of these ordered planes in subsequent layers are possible. For example, Fig. 3 shows two possible stacking variants of the ordered phases with $x=0.25$. Large and small filled circles indicate different lithium planes. For the ordering at $x=\frac{1}{3}$ and at $x=\frac{2}{3}$ shown in Fig. 2(b) only one variant is possible.

In this paper we demonstrate that Li_xNiO_2 and Li_xCoO_2 consistently choose a different stacking variant for the Li-ordered planes. In Li_xCoO_2 the stacking is chosen so as to minimize the variations in coordination of the symmetrically

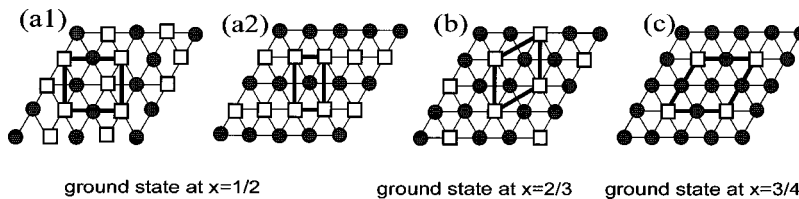


FIG. 2. In-plane lithium ordering in Li_xMO_2 at $x=(a) \frac{1}{2}$, (b) $\frac{2}{3}$, and (c) $\frac{3}{4}$. Circles represent the sites occupied by lithium ions and squares are vacant sites. If the circles are denoted as vacancies and the squares as Li ions, then (b) refers to Li ordering at $x=\frac{1}{3}$ and (c) refers to Li ordering at $x=\frac{1}{4}$.

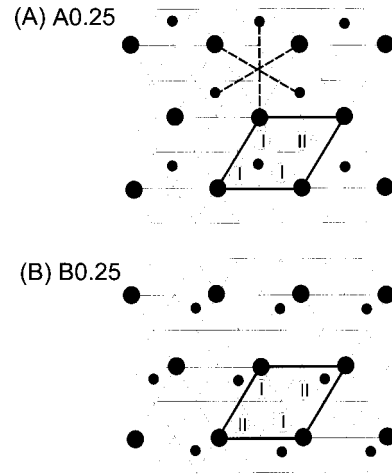


FIG. 3. Two different stacking sequences of the Li ordering in Fig. 2(c) for a $\text{Li}_{0.25}\text{MO}_2$ compound in the (a) A0.25 structure and (b) B0.25 structure. Filled small circles represent lithium ions in the next plane, and open circles M ions. The unit cell is indicated with a bold line and the M sites indicated as I and II.

different Co sites, whereas the opposite occurs in Li_xNiO_2 . In Li_xNiO_2 , lithium ordering couples to orbital and Jahn-Teller ordering so as to form $180^\circ \text{Li-O-Ni}^{+3}\text{-O-Li}$ complexes. The selection of stacking will be shown to be driven by the electronic structure of the transition-metal cations (metallic for $\text{Co}^{+3/+4}$, localized for $\text{Ni}^{+3/+4}$).

II. METHOD

To calculate the internal energy of Li_xMO_2 compounds we used the *ab initio* pseudopotential method as implemented in the Vienna *Ab initio* Simulation Package (VASP).^{16,17} This method solves the Kohn-Sham equations within the local density (LDA) or the generalized gradient approximation (GGA) using ultrasoft pseudopotentials. Calculations were performed within the generalized gradient approximation as GGA was found to be essential for correctly reproducing the Jahn-Teller distortion in LiMnO_2 , LiNiO_2 , and LiCuO_2 .^{13,18} A plane-wave basis set with a kinetic-energy cutoff of 400 eV was used, which is adequate for these structures. The reciprocal space sampling was done in a $6 \times 6 \times 6$ k -point grid for structures containing two LiMO_2 formula units, and in a $4 \times 4 \times 4$ k -point grid for larger supercells. Relaxation was allowed and the final energies of the optimized geometries were recalculated so as to correct for changes in basis during relaxation. Li_xMO_2 structures were

TABLE I. Bond lengths and oxidation states for $\text{Li}_{0.25}\text{MO}_2$ in the A0.25 and B0.25 structures.

Structure	M ion	Number of atoms (%)	Average M -O distance (\AA)	Oxidation state
A0.25	Ni(I)	75	1.8937	+4
	Ni(II)	25	1.9619	+3.2
B0.25	Ni(I)	50	1.8933	+4
	Ni(II)	50	1.9237	+3.7
A0.25	Co(I)	75	1.8876	charge
	Co(II)	25	1.9092	delocalization
B0.25	Co(I)	50	1.8889	charge
	Co(II)	50	1.8993	delocalization

studied at x values of $\frac{2}{3}$, $\frac{1}{2}$, $\frac{1}{3}$, and $\frac{1}{4}$ taking supercells of up to four LiMO_2 formula units. In Li_xNiO_2 the energy of 14 structures was calculated at $x=0.25$ and 0.5, while eight structures were considered at $x=\frac{1}{3}$ and $\frac{2}{3}$. For Li_xCoO_2 compounds the energy of 9 structures were calculated. Finally, in Li_xMnO_2 only some particular configurations were studied.

III. RESULTS AND DISCUSSION

A. Ground states at $x=0.25$ and 0.5

1. $\text{Li}_{0.25}\text{MO}_2$

An energetically favorable configuration for Li-vacancy configuration in a plane at $x=0.25$ is that of Fig. 2(c). The stability of this structure can easily be understood since, consistent with repulsive interactions, it puts individual Li ions as far apart as possible. Two possible stacking sequences of successive lithium planes are possible (Fig. 3). We refer to this as A0.25 and B0.25. Table I summarizes the calculated M -O distance data for the M octahedra in the two structures, and an approximate value for the Ni oxidation state obtained by integrating the spin-polarization density up to a 2 \AA radius around each Ni ion is given.

In the A0.25 structure two distinct M ions are present, M (I) and M (II), in a 3:1 ratio. M (I) has the shorter bond lengths to oxygen, indicative of a higher positive valence than M (II). However, in the case of Li_xCoO_2 , the average distance of Co(I) and Co(II) to oxygen is too similar to assign them different oxidation states. This fact already indicates a strong charge delocalization in this compound. On the contrary, the difference in average M -O distances for Ni(I) and Ni(II) ions is large, suggesting the existence of localized Ni^{+3} and Ni^{+4} ions. We have confirmed this by integrating the spin-polarization density around each Ni ion (see Table I). Figure 4(a) shows the total electron-spin difference, taken as the electron spin up minus the electron spin down as a function of the integration radius around Ni. The Ni(I) ion has a filled (t_{2g})⁶ shell with no net electron spin, whereas Ni(II) has approximately one net electron spin. This implies that Ni(II) is a Ni^{+3} ion and Ni(I) is a Ni^{+4} ion. This may at first be surprising since Ni(I) is more closely coordinated by Li^+ ions than Ni(II). Pure electrostatic charge-compensation consideration would therefore favor Ni(I) to

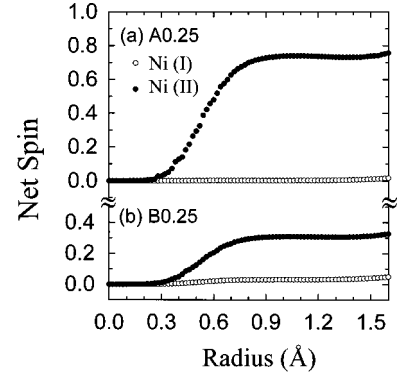


FIG. 4. Net electron spin around Ni in $\text{Li}_{0.25}\text{NiO}_2$ as a function of the integration radius in the (a) A0.25 structure and (b) B0.25 structure.

have a lower positive valence charge. However, as we will show later, important interplane $\text{Li}_A\text{-O-Ni-O-Li}_B$ interactions explain this unusual behavior.

In the B0.25 structure two distinct M ions are present, but in a 1:1 ratio. Co(I) and Co(II) have even closer average M -O distances than in the A0.25 structure. The valence states of the Ni ions can again be inferred from the Ni-O distance and from the electron-spin difference shown in Fig. 4(b). Ni(I) has a slightly net electron spin (effectively 0.02), suggesting that it is a Ni^{+4} ion. Ni(II) with 0.3 electrons in the e_g orbital is approximately a $\text{Ni}^{+3.7}$ ion. Consequently, in B0.25 no Jahn-Teller active Ni^{+3} is present.

Regarding the relative stability of these structures, the energy of A0.25 is about 5 meV *below* that of B0.25 for $\text{Li}_{0.25}\text{NiO}_2$, whereas it is 18 meV *above* B0.25 for $\text{Li}_{0.25}\text{CoO}_2$. Hence $\text{Li}_{0.25}\text{NiO}_2$ prefers as ground state the structure A0.25, where electronic charge localization and therefore Jahn-Teller-active Ni^{+3} ions are possible. $\text{Li}_{0.25}\text{CoO}_2$ prefers the B0.25 ordering to the A0.25, since the former favors a better charge delocalization.

2. $\text{Li}_{0.5}\text{MO}_2$

Figure 2(a) show the most likely lithium-vacancy in-plane ordered arrangements at $x=0.5$. The ordered arrangement in Fig. 2(a2) is a potential ground state when considering only repulsive interactions up to second neighbor. The ordered arrangement in Fig. 2(a1) becomes a potential ground state when a third-neighbor interaction is introduced.¹⁹ Figures 5(a) and 5(b) correspond to the two possible stacking sequences taking the in-plane ordering of Fig. 2(a2) denoted as structures A0.5 and B0.5, respectively. Table II shows some M -O data corresponding to $\text{Li}_{0.5}\text{NiO}_2$ and $\text{Li}_{0.5}\text{CoO}_2$ in each of these structures. In Li_xNiO_2 the oxidation state has been obtained by spin difference integration up to a 2 \AA radius around Ni ions.

Structure A0.5 has two types of M ions in a ratio 1:1, whereas B0.5 has only one distinct M site. In the structure A0.5 for $M=\text{Co}$, both Co(I) and Co(II) have similar average Co-O distances, reflecting electronic charge delocalization. For $M=\text{Ni}$ different Ni-O bond lengths occur. As indicated from the average Ni-O distance, and confirmed by the spin

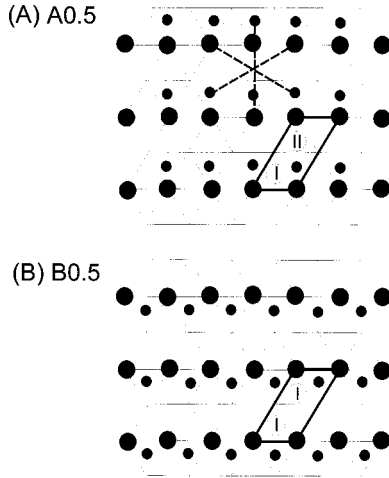


FIG. 5. Stacking sequences for the in-plane lithium ordering shown in Fig. 2(a). (a) Structure A0.5 and (b) structure B0.5. Filled small circles represent lithium ions in the plane above, and open circles M ions. The unit cell is denoted with a bold line and the M sites indicated as I and II.

difference integrations [see Fig. 6(a)], Ni(II) is a Ni^{+3} ion and Ni(I) is a Ni^{+4} ion in the A0.5 structure. In the structure B0.5 there is only one type of M site, so the M valence state should be $+3.5$. Figure 6(b) shows the total electron-spin difference for $\text{Li}_{0.5}\text{NiO}_2$ in the B0.5 structure. A net spin of 0.4 electrons indicates a $\text{Ni}^{+3.6}$ ion.

Regarding the relative stability of these two structures, in $\text{Li}_{0.5}\text{NiO}_2$, structure A0.5 is 26 meV *below* structure B0.5. This energetic stability is reversed in $\text{Li}_{0.5}\text{CoO}_2$ where structure B0.5 is more stable than A0.5 by 33 meV. Consistent with the observation in $\text{Li}_{0.25}\text{MO}_2$, the nature of the M ions

TABLE II. Bond lengths and oxidation states for $\text{Li}_{0.5}\text{MO}_2$ in the A0.5, B0.5, C0.5, D0.5, and E0.5 structures.

Structure	M ion	Number of atoms (%)	Average M -O distance (\AA)	Oxidation state
A0.5	Ni(I)	50	1.8956	+4
	Ni(II)	50	1.9696	+3.2
B0.5	Ni(I)	100	1.9283	+3.6
C0.5	Ni(I)	50	1.9059	+3.9
	Ni(II)	50	1.9561	+3.3
D0.5	Ni(I)	50	1.9132	+3.85
	Ni(II)	25	1.9442	+3.4
	Ni(III)	25	1.9491	+3.4
E0.5	Ni(I)	100	1.9289	+3.6
A0.5	Co(I)	50	1.8925	charge
	Co(II)	50	1.9140	delocalization
B0.5	Co(I)	100	1.9054	formal +3.5
C0.5	Co(I)	50	1.8998	charge
	Co(II)	50	1.9044	delocalization
D0.5	Co(I)	50	1.9013	charge
	Co(II)	25	1.9004	delocalization
	Co(III)	25	1.9017	
E0.5	Co(I)	100	1.9029	formal +3.5

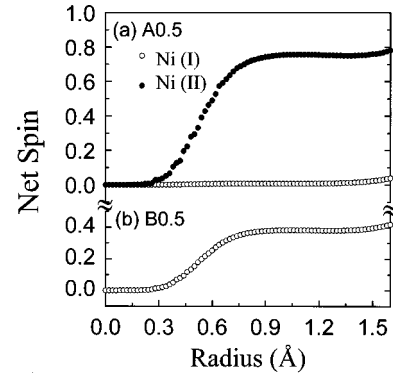
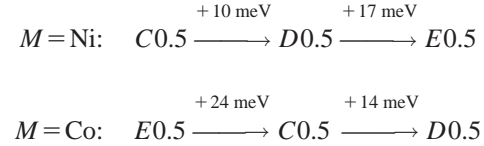


FIG. 6. Net electron-spin difference around Ni in $\text{Li}_{0.5}\text{NiO}_2$ as a function of the integration radius in the (a) A0.5 structure and (b) B0.5 structure.

determines the ground state. Co ions prefer stacking sequences that result in equivalent environments for all the Co ions. This ensures maximal charge delocalization (structure B0.5). Ni ions rather adopt structures with distinct M sites, which allow charge localization (JT effect). Thus electronic properties of M are the driving force in stabilizing a particular Li_xMO_2 structure.

This dependence of the structural stability with the electronic nature of the transition metal is confirmed for any other in-plane ordering. We could consider, for example, the in-plane ordering of Fig. 2(a1) for which three possible stacking sequences are possible. These are denoted as structures C0.5, D0.5, and E0.5 in Fig. 7 and Table II. The energetic stability of these three $\text{Li}_{0.5}\text{MO}_2$ structures depends on the nature of M as follows:



This points out once more the tendency for Co ions to delocalize the electronic charge, and for Ni ions to localize it.

B. Out-of-plane Li-Li interactions

In the previous section we considered Li_xMO_2 structures with the same in-plane lithium-vacancy ordering but different stacking sequences (A0.25-B0.25, A0.5-B0.5, and C0.5-D0.5-E0.5). Changing the stacking sequence implies an alteration of the environments around M sites. Hence the preference of the M ion for a particular environment determines the stacking sequence. This site selection depends on the electronic characteristics of M : charge localization (delocalization) needs distinct (equivalent) M sites. The next question to solve is how the environment of M sites acts to localize or delocalize electronic charge. Since the studied structures differ only in the stacking sequence of Li-vacancy planes, this matter has to be obviously related to some Li-Li interplane interactions.

The schematic representation of the LiMO_2 structure in Fig. 1 shows two planes of lithium ions (A and B). We will

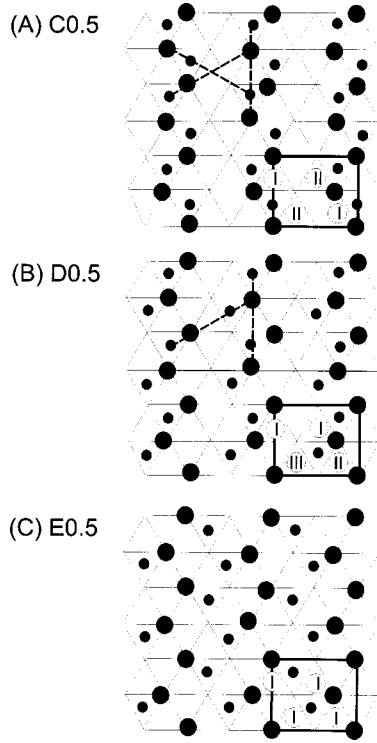


FIG. 7. Possible ordered structures in $\text{Li}_{0.5}\text{MO}_2$ with the in-plane ordering shown in Fig. 2(a1). (a) Structure C0.5, (b) structure D0.5, and (c) structure E0.5. The filled small circles represent lithium ions in the plane above, and open circles M ions. The unit cell is denoted with a bold line and the M sites indicated as I and II.

discuss the $\text{Li}_A\text{-Li}_B$ interaction through a particular M ion, whose $M\text{-O}$ octahedra is indicated in Fig. 1. In an octahedral environment, the five d orbitals of a transition-metal atom are no longer degenerate, but split in two groups, the t_{2g} group (d_{xy}, d_{yz}, d_{xz}) pointing away from oxygen atoms, and the e_g group ($d_{x^2-y^2}, d_{z^2}$). The latter overlap directly with the $p_x, p_y,$ and p_z oxygen orbitals forming bonding e_g bands and antibonding e_g^* bands. The antibonding e_g^* bands are predominantly d in character, and lie above the t_{2g} bands. Each oxygen at the vertex of an M octahedron is also connected through the $2p_x, 2p_y,$ and $2p_z$ orbitals to the $2s$ orbital of a lithium ion. Hence if the Li site is occupied, that lithium ion shares an $\text{O-}2p$ orbital with M . This multiple bonding $M\text{-(}3d\text{)-O-(}2p\text{)-Li-(}2s\text{)}$ is represented in Fig. 8. The six lithium ions interacting in this way with the e_g orbitals ($d_{x^2-y^2}$ and d_{z^2}) of the central M ion are indicated by the upward pointing triangles in Fig. 1. We argue that these orbitals in Li_xNiO_2 generate attractive interactions between Li ions in $180^\circ \text{Li}_A\text{-O-}M\text{-O-Li}_B$ configurations. The arguments for such attractive interactions will be made in two parts: (1) the presence of Li at the extension of a $M\text{-O}$ bond lowers the energy of that e_g^* orbital and (2) the ability of the M ion to Jahn-Teller distort leads, in a system with noninteger metal valence, to charge localization in filled and unfilled orbitals.

$\text{Li-}2s, \text{O-}2p,$ and metal $d_{x^2-y^2}, d_{z^2}$ orbitals have the proper symmetry to hybridize. Our results suggest that the presence of Li ions at the extension of a $M\text{-O}$ bond lowers

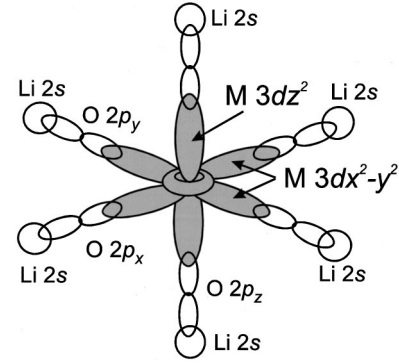


FIG. 8. Overlapping of atomic orbitals involved in the $\text{Li}_A\text{-O-}M\text{-O-Li}_B$ interactions.

the energy of that e_g^* orbital. For this reason, as we will demonstrate in subsequent sections, the Li ions in Li_xNiO_2 prefer second-neighbor positions to the Ni^{3+} ions. The s -orbital of Li forms a σ overlap with the e_g^* of its second nearest neighbor Ni but not with its first nearest neighbor (NN) Ni. Hence the presence of lithium lowers the e_g^* of its second NN Ni, making it lower in valence than its first NN Ni. However, every Li site can form a σ overlap with some second NN Ni ions and it remains to be explained why this leads to favoring particular interplane Li-Li interactions. We now argue that attractive $180^\circ \text{Li}_A\text{-O-}M\text{-O-Li}_B$ interactions are created by the Jahn-Teller instability of the e_g^* orbitals.

In the simplest description for the Jahn-Teller distortion²⁰ the energy of an isolated center consists of two parts: an electronic term that is linear in the distortion (δ) and an elastic term that varies quadratic with the distortion

$$E = \lambda \delta + B \delta^2.$$

It can easily be deduced that in this model the Jahn-Teller stabilization energy scales quadratically with the electron-phonon coupling parameter (λ)

$$E_{JT} \propto \lambda^2 / B.$$

If we assume that a half-filled spin orbital corresponds to about half the strength of λ of a filled spin orbital, a system with two $\text{Ni}^{3.5}$ ions would only generate half the Jahn-Teller distortion energy than the combination of a Ni^{+3} and a Ni^{+4} . Through its quadratic dependence on orbital filling, the Jahn-Teller distortion therefore provides a mechanism for charge localization. This leads to attractive interplanar Li interactions whenever those Li ions hybridize with the same e_g^* orbital, i.e., whenever they form a $180^\circ \text{Li}_A\text{-O-}M\text{-O-Li}_B$ configuration. This follows from the argument that hybridization of two Li ions with the same e_g^* orbital lowers the energy of that orbital, allowing it to be completely filled, and hence obtain maximum benefit of the Jahn-Teller distortion. In the case when two of the 180° positions around a Ni ion are occupied with Li and the other four are empty, it can be expected that the d_{z^2} orbital is filled and oriented along the $\text{Li}_A\text{-O-}M\text{-O-Li}_B$ directions. The Ni ion would be in a mode of positive Jahn-Teller distortion (two long and four short bonds). In the case of four Li ions (two 180° pairs) around

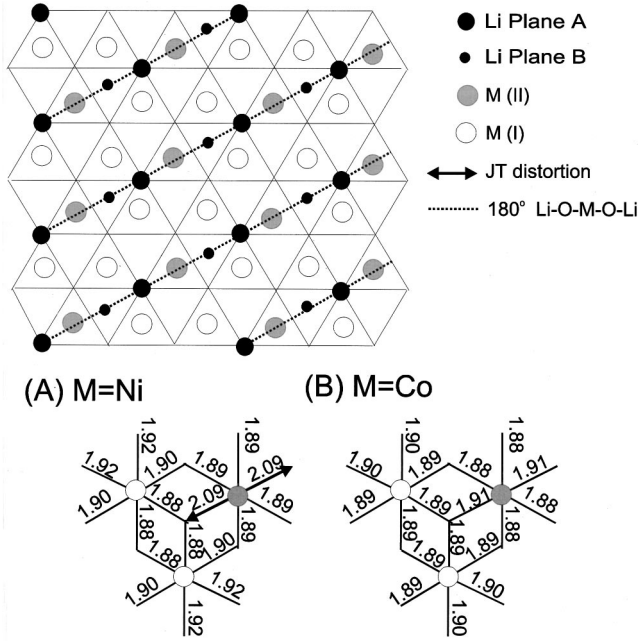


FIG. 9. Representation of the cationic arrangement and M -O distances in the $\text{Li}_{1/3}\text{MO}_2$ ground state for (a) $M=\text{Ni}$ and (b) $M=\text{Co}$. Average M -O distances are $\text{Ni(I)-O}=1.90 \text{ \AA}$, $\text{Ni(II)-O}=1.96 \text{ \AA}$, $\text{Co(I)-O}=1.89 \text{ \AA}$, and $\text{Co(II)-O}=1.89 \text{ \AA}$.

Ni, the $d_{x^2-y^2}$ orbital will hybridize with the $\text{Li-}2s$ orbitals. Its filling will lead to a negative Jahn-Teller distortion (four long and two short bonds). The presence of six Li ions (all 180° pairs filled) will lower both e_g^* orbitals, but may still lead to a Jahn-Teller distortion, as is predicted for LiNiO_2 . Since with six second-neighbor Li ions the Jahn-Teller distortion is not assisted by the Li hybridization, the distortion is expected to be somewhat smaller in magnitude.

In Li_xCoO_2 the situation is different as its e_g^* orbitals are empty. Hybridization of the e_g^* orbitals with $\text{Li-}2s$ orbitals will, therefore, not affect the energy, and the system will not have the attractive $180^\circ \text{Li}_A\text{-O-M-O-Li}_B$ interactions.

C. $\text{Li}_A\text{-O-M-O-Li}_B$ interactions and JT distortion

In this section we will demonstrate that the attractive $180^\circ \text{Li}_A\text{-Li}_B$ interaction across a transition-metal center couples to the Jahn-Teller distortion. As argued above, the presence of these $\text{Li}_A\text{-O-M-O-Li}_B$ interactions leads to the preferential filling of some e_g^* orbitals, hence charge localization and an associated JT distortion.

First we will examine the ground states at $x=\frac{1}{3}$ and $\frac{2}{3}$ where no different stacking of the stable in-plane ordering is possible. Later we will discuss the structures A0.25 and C0.5, which are the most stable in the Li_xNiO_2 system. All these structures are represented in Figs. 9–12, which show the location of distinct M sites (between two successive lithium layers), the distances to their six nearest-neighbor oxygen ions, the direction of the JT distortion, and the $180^\circ \text{Li}_A\text{-O-M-O-Li}_B$ configurations.

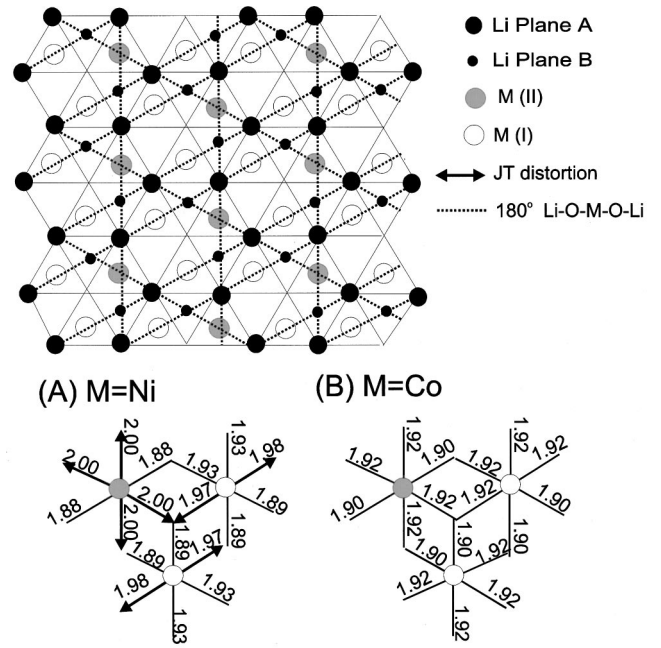


FIG. 10. Representation of the cationic arrangement and M -O distances in the $\text{Li}_{2/3}\text{MO}_2$ ground state in (a) $\text{Li}_{2/3}\text{NiO}_2$ and (b) $\text{Li}_{2/3}\text{CoO}_2$. Average M -O distances are $\text{Ni(I)-O}=1.93 \text{ \AA}$, $\text{Ni(II)-O}=1.97 \text{ \AA}$, $\text{Co(I)-O}=1.91 \text{ \AA}$, and $\text{Co(II)-O}=1.92 \text{ \AA}$.

I. $\text{Li}_{1/3}\text{MO}_2$

Figure 9 shows the representation of this structure with the M -O distances in (a) $M=\text{Ni}$ and (b) $M=\text{Co}$. Two different types of M atoms are present in a ratio 2:1. In $\text{Li}_{1/3}\text{NiO}_2$ the M -O distances, as well as the integrated spin density, indicate that Ni(II) is a Ni^{+3} JT distorted ion. Ni^{+3} ions sit in

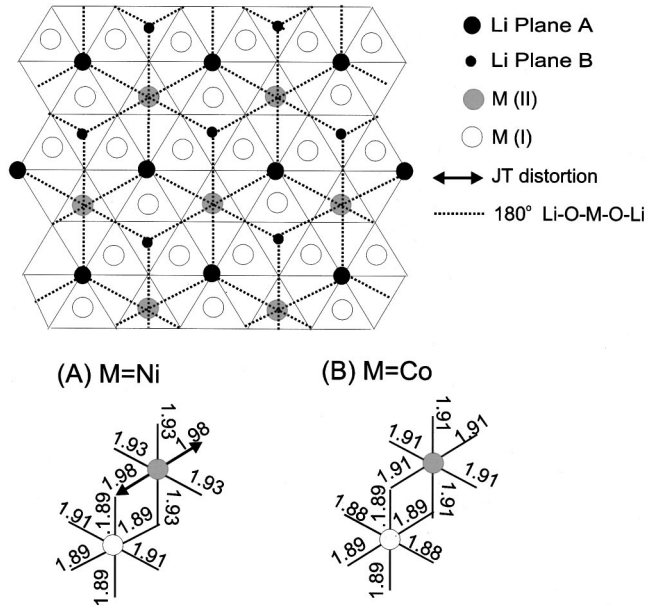


FIG. 11. Representation of the cationic arrangement in the A0.25 structure and M -O distances distribution in (a) $\text{Li}_{0.25}\text{NiO}_2$ and (b) $\text{Li}_{0.25}\text{CoO}_2$. Average M -O distances are $\text{Ni(I)-O}=1.89 \text{ \AA}$, $\text{Ni(II)-O}=1.96 \text{ \AA}$, $\text{Co(I)-O}=1.89 \text{ \AA}$, and $\text{Co(II)-O}=1.91 \text{ \AA}$.

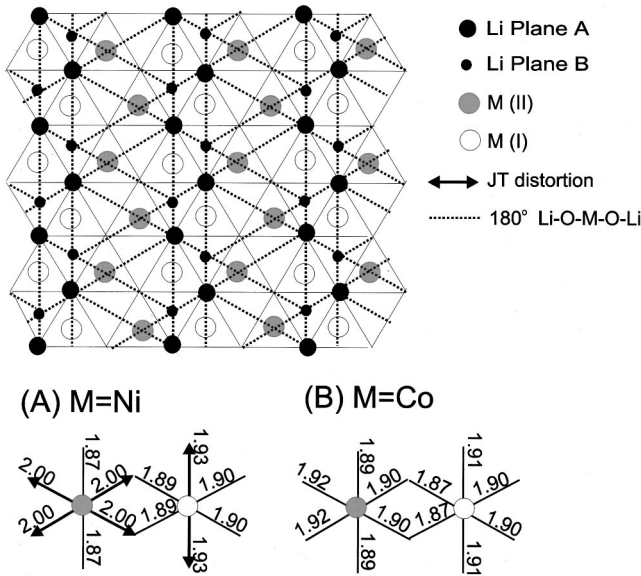


FIG. 12. Representation of the cationic arrangement in the C0.5 structure and M -O distances distribution in (a) $\text{Li}_{0.5}\text{NiO}_2$ and (b) $\text{Li}_{0.5}\text{CoO}_2$. Average M -O distances are $\text{Ni(I)-O} = 1.91 \text{ \AA}$, $\text{Ni(II)-O} = 1.96 \text{ \AA}$, $\text{Co(I)-O} = 1.90 \text{ \AA}$, and $\text{Co(II)-O} = 1.90 \text{ \AA}$.

elongated octahedra with $(4+2)$ coordination. The longest Ni(II)-O bonds (2.09 \AA) are pointing towards Li atoms in the plane above and below, forming a $\text{Li}_A\text{-O-M-O-Li}_B$ chain with a $\text{Li}_A\text{-M-Li}_B$ angle of 180° . In the other four equivalent Ni(II)-O directions, where the Ni(II)-O bond length is 1.89 \AA , this position is a vacancy, resulting in $\square\text{-O-M-O-}\square$ chains. As commented on in Sec. III B this situation corresponds to the local filling of the $M d_{z^2}$ orbital, hence the JT axis is lined up with the $\text{Li}_A\text{-O-M-O-Li}_B$ configurations. The elongated $\text{Ni}^{+3}\text{-O}$ bonds are aligned in the structure resulting in a cooperative Jahn-Teller distortion. The Ni I ion has several NN Li positions filled but no second NN (i.e., no 180° pairs). Hence it does not benefit from hybridization with Li- s and is a Ni^{+4} ion in agreement with its shorter bond lengths. In the case of $\text{Li}_{1/3}\text{CoO}_2$ all bond lengths are similar.

2. $\text{Li}_{2/3}\text{MO}_2$

In $\text{Li}_{2/3}\text{NiO}_2$ [Fig. 10(a)] two distinct types of Ni ions, labeled as Ni(I) and Ni(II), are present in a ratio 2:1. Both Ni-O distances and spin charge integration indicate that Ni(I) is a $\text{Ni}^{+3.5}$ ion, whereas Ni(II) is a Ni^{+3} ion. Ni(II) has four Li ions in second NN positions (two 180° pairs). Hence the $d_{x^2-y^2}$ orbital is filled and a negative Jahn-Teller distortion takes place around this ion (four long and two short Ni-O bond lengths). Because Ni I is a $\text{Ni}^{+3.5}$, it may have weak Jahn-Teller activity. This seems to be the case, as can be observed by the longer bond lengths in the direction of the 180° Li pair. Again, in the equivalent Co structure all bond lengths are similar.

3. $\text{Li}_{0.25}\text{MO}_2$ in the A0.25 structure

The lowest-energy configuration of $\text{Li}_{0.25}\text{NiO}_2$ is represented in Fig. 11. Surprisingly, in spite of the lower lithium

content, Ni(II) is surrounded by six lithium ions forming three $\text{Li}_A\text{-O-Ni-O-Li}_B$ chains. This leads to a weak JT distortion of this octahedron. Consequently this cooperative JT distortion gives rise to a monoclinic $\text{Li}_{0.25}\text{NiO}_2$. As can be seen in Fig. 11(b), replacing Ni by Co in this structure suppresses the monoclinic distortion, giving a rhombohedral compound (space group $R\bar{3}m$).

4. $\text{Li}_{0.5}\text{MO}_2$ in the C0.5 structure

Figure 12 shows the C0.5 ground-state configuration. The M -O distance distribution in $\text{Li}_{0.5}\text{NiO}_2$ fully responds to the expectations from the lithium arrangement. Two 180° $\text{Li}_A\text{-O-Ni-O-Li}_B$ chains around Ni(II) stabilizes a negative JT distorted Ni^{+3} octahedra (occupation of the $d_{x^2-y^2}$ orbital), and one 180° $\text{Li}_A\text{-O-Ni-O-Li}_B$ chain stabilizes a slightly distorted Ni^{+4} octahedra. The corresponding $\text{Li}_{0.5}\text{CoO}_2$ does not have such different Co-O bond lengths.

D. Confirmation in Li_xMnO_2

In the previous section we have shown that interplane lithium ordering allowing 180° $\text{Li}_A\text{-O-M-O-Li}_B$ leads to distinct M sites favoring electronic charge localization and local or cooperative Jahn-Teller distortions. Absence of these interactions favors charge-delocalized Li_xMO_2 structures where the M ions are as equivalent as possible. Up to now we have demonstrated this with the Li_xNiO_2 and Li_xCoO_2 systems. In order to generalize the rules controlling the stability of ordered Li_xMO_2 , these criteria should also apply to other Li_xMO_2 systems. Among other possible Li_xMO_2 compounds we focus on $\text{Li}_{0.5}\text{MnO}_2$ with the different stacking sequences shown in Fig. 5.

Since Mn^{+3} in its high spin (HS) configuration ($t_{2g}^3 e_g^1$) is a strong JT-active ion, confirmation of the 180° interaction JT distortion coupling can be found in $\text{Li}_{0.5}\text{MnO}_2$ structures (Fig. 5). As expected from Sec. III A 2, structure B0.5 with no 180° interactions provides only one type of Mn site, and there is no possibility to localize the electronic charge (no JT-active Mn^{+3}). Structure A0.5 possesses 180° interactions that allow the presence of JT distorted HS Mn^{+3} . The calculated energies for $\text{Li}_{0.5}\text{MnO}_2$ indicate that structure A0.5 is more stable than structure B0.5 by 84 meV . Thus, the order of relative stability is the same as in $\text{Li}_{0.5}\text{NiO}_2$ but the differences in energy are larger in $\text{Li}_{0.5}\text{MnO}_2$, likely due to the stronger JT effect of HS Mn^{+3} . Features in ordered Li_xMnO_2 therefore corroborate those observed in the Li_xNiO_2 system.

Furthermore the analysis of $\text{Li}_{0.5}\text{MnO}_2$ can bring new insights by examining the relative energy of the A0.5 and B0.5 structures for low spin Mn^{+3} (t_{2g}^4). These energies have been calculated by forcing Mn^{+3} electronic configuration to be low spin (LS) ($t_{2g}^4 e_g^0$). In this way the JT distortion is eliminated and Mn should behave similar to Co, in the sense that electronic states tend to delocalize. Effectively, the energy of $\text{Li}_{0.5}\text{Mn}^{\text{LS}}\text{O}_2$ in the B0.5 structure is 20 meV lower than that of the A0.5 structure. Suppression of the JT distortion reverses the stability of the structures, making the stacking sequence without 180° $\text{Li}_A\text{-O-M-O-Li}_B$ interactions more stable. This demonstrates that non-JT-active M ions

prefer to sit in equivalent sites that allow electronic charge delocalization. The features observed in ordered $\text{Li}_x\text{Mn}^{\text{LS}}\text{O}_2$ corroborate those observed in Li_xCoO_2 system.

IV. CONCLUSIONS

Our results show that the electronic nature of M plays a dominant role in determining the relative stability between different ordered structures. While short-range electrostatic interactions dominate the Li arrangement in the lithium plane, the stacking sequence of these planes in layered Li_xMO_2 is determined by the electronic nature of the transition-metal ion. Metallic properties of Co and Mn^{LS} lead to ground states where the M sites are nearly equivalent, so the delocalization of charge is possible. On the contrary, the charge localization in Li_xNiO_2 and Li_xMnO_2 is favored when M^{+3} and M^{+4} sites have different environments. In Li_xNiO_2 and Li_xMnO_2 we find evidence for an important attractive interaction between Li planes even though they are separated by 5 Å. In fact the distance between Li_A and Li_B in a $\text{Li}_A\text{-O-M-O-Li}_B$ chain is around 8.5 Å. An occupied e_g^* spin orbital in these compounds can lower its energy by hybridization with a Li $2s$ orbital. Since the energy of Jahn-Teller distortion is largest when charge is localized in completely filled spin orbitals, Li ions will preferentially hybridize with the same e_g^* orbital. Hence the combined effect of $e_g^*\text{-Li-}2s$ overlap with the Jahn-Teller activity of the Ni or Mn ion leads to attractive Li interactions across 180° $\text{Li}_A\text{-O-M-O-Li}_B$ connections. We found that all Li_xNiO_2 structures that have such 180° Li pairs have lower energy than structures without these configurations but with the same in-plane lithium ordering. One 180° $\text{Li}_A\text{-O-M-O-Li}_B$ leads to filling of the d_{z^2} orbital and a positive Jahn-Teller distortion across the Ni ions. When two orthogonal 180° $\text{Li}_A\text{-O-M-O-Li}_B$ pairs exist over the Ni ion, the $d_{x^2-y^2}$ is filled, resulting in a negative Jahn-Teller distortion. In Li_xCoO_2 no coupling between e_g^* and Li- $2s$ occurs

and the lowest-energy interplanar stackings are those that lead to Co sites that are as equivalent as possible. This is consistent with a $\text{Co}^{+3}/\text{Co}^{+4}$ tendency for charge delocalization, as is observed in this material.²¹

Transition-metal induced attractive interactions between ions have been observed before. For example, in $\text{YBa}_2\text{Cu}_3\text{O}_{6+x}$, hybridization between Cu and O orbitals leads to the attractive interactions that produce the characteristic defect chain structures in this material.²²

In conclusion, we have shown that coupling between Li ordering, Ni-valence ordering, and Jahn-Teller distortions in Li_xNiO_2 compounds gives rise to attractive Li-Li interactions. Evidence of these results through experiments is limited. Experiments are performed at finite temperatures so one has to be aware of the possibility that the transition temperature of an ordered state could be below the temperature of the experiment. If this were the case, no ordered state would be detected. There is also the possibility that a new structure may appear at finite temperatures as an intermediate phase between the ordered structure and the disordered one. If so, the experimentally detected ordered structure could be different from those reported in this work. At this point, Li_xMO_2 phase diagrams are crucial in determining the temperature stability of the ordered ground states. The Li_xCoO_2 phase diagram has already been reported,⁵ and the Li_xNiO_2 one is currently in progress. Further experimental efforts are also required since, as far as we know, experimental proposed models^{4,23,24,25} only examine the in-plane lithium ordering. This neglects the important interplane interaction and restricts possible comparison to the presented calculations.

ACKNOWLEDGMENTS

This work was supported by the Department of Energy under Grant No. DE-FG02-96ER45571. G.C. acknowledges support from Union Minière in the form of a Faculty Development Chair. One of the authors (M.E. y d.D.) thanks Universidad Complutense de Madrid for partial support.

¹G. Ceder, A. Van der Ven, C. Marianetti, and D. Morgan, *Modell. Simul. Mater. Sci. Eng.* **8**, 311 (2000).

²E. J. Wu, P. D. Tepesch, and G. Ceder, *Philos. Mag. B* **77**, 1039 (1998).

³J. N. Reimers and J. R. Dahn, *J. Electrochem. Soc.* **139**, 2091 (1992).

⁴J. P. Peres, F. Weill, and C. Delmas, *Solid State Ionics* **116**, 19 (1999).

⁵A. Van der Ven, M. K. Aydinol, G. Ceder, G. Kresse, and J. Hafner, *Phys. Rev. B* **58**, 2975 (1998).

⁶K. Mizushima, P. C. Jones, P. J. Wiseman, and J. B. Goodenough, *Mater. Res. Bull.* **15**, 783 (1980).

⁷A. R. Armstrong and P. G. Bruce, *Nature (London)* **381**, 499 (1996).

⁸J. B. Goodenough, D. G. Wickham, and W. J. Croft, *J. Phys. Chem. Solids* **5**, 107 (1958).

⁹C. Delmas, M. Menetrier, L. Croguennec, S. Levasseur, J. P. Peres, C. Pouillier, G. Prado, L. Fournes, and F. Weill, *Int. J.*

Inorg. Mater. **1**, 11 (1999).

¹⁰M. G. S. R. Thomas, W. I. F. David, J. B. Goodenough, and P. Groves, *Mater. Res. Bull.* **20**, 1137 (1985).

¹¹J. Morales, C. Perez-Vicente, and J. L. Tirado, *Mater. Res. Bull.* **25**, 623 (1990).

¹²A. Rougier, C. Delmas, and A. V. Chadwick, *Solid State Commun.* **94**, 123 (1995).

¹³C. Marianetti, D. Morgan, and G. Ceder, *Phys. Rev. B* (to be published).

¹⁴M. Kaburagi and J. Kanamori, *Jpn. J. Appl. Phys., Suppl.* **2**, 145 (1974).

¹⁵G. Ceder and A. Van der Ven, *Electrochim. Acta* **45**, 131 (1999).

¹⁶G. Kresse and J. Furthmüller, *Phys. Rev. B* **54**, 11 169 (1996).

¹⁷G. Kresse and J. Furthmüller, *Comput. Mater. Sci.* **6**, 15 (1996).

¹⁸S. K. Mishra and G. Ceder, *Phys. Rev. B* **59**, 6120 (1999).

¹⁹M. Kaburagi and J. Kanamori, *J. Phys. Soc. Jpn.* **44**, 718 (1978).

²⁰I. B. Bersuker, in *Electronic Structure and Properties of Transi-*

- tion Metal Compounds* (John Wiley & Sons, Inc., New York, 1996).
- ²¹M. Menetrier, I. Saadoune, S. Levasseur, and C. Delmas, *J. Mater. Chem.* **9**, 1135 (1999).
- ²²D. de Fontaine, L. T. Wille, and S. C. Moss, *Phys. Rev. B* **36**, 5709 (1987).
- ²³A. Ueda and T. Ohzuku, *J. Electrochem. Soc.* **141**, 2010 (1994).
- ²⁴H. Arai, S. Okada, H. Ohtsuka, M. Ichimura, and J. Yamaki, *Solid State Ionics* **80**, 261 (1995).
- ²⁵C. Delmas, J. P. Peres, A. Rougier, A. Demourges, F. Weill, A. Chadwick, M. Broussely, F. Perton, Ph. Biensan, and P. Willmann, *J. Power Sources* **68**, 120 (1997).